ACS OMEGA

http://pubs.acs.org/journal/acsodf

Article

Synthesis and Characterization of a Titanium-Based Functionally Graded Material-Structured Biocomposite using Powder Metallurgy

Ehsan Ul Haq, Furqan Ahmed, Faseeh U Rehman, Iftikhar Ahmed Channa, Muhammad Atif Makhdoom, Junaid Shahzad, Tooba Shafiq, Muhammad Zain-ul-Abdein,* Muhammad Ali Shar, and Abdulaziz Alhazaa

Cite This: *ACS Omega* 2023, 8, 28976−28983

Read Online

ACCESS | Metrics & More | Article Recommendations

ABSTRACT: This investigation aims at synthesizing and characterizing a biocomposite of hydroxyapatite (HA) and titanium (Ti) as a functionally graded material (FGM) via an economical powder metallurgy route. Ti particles were produced through drilling and chipping, followed by compaction and sintering. Ti foams, so obtained, were then infused with varying volume fractions of HA. The pure Ti foam control sample and the FGM composite samples were then subjected to various characterizations to validate their biocompatibility, structural strength, and integrity. The interface development between the load-bearing Ti implant and living tissue was resolved through an FGM structure, where the base of the implant consisted of load-bearing Ti and the outer periphery changed to HA gradually. HA/Ti specimens of different volume fractions were tested for density measurements, microstructure, hardness, and bioactivity. The bioactive behavior was investigated using the potentiodynamic polarization technique to measure the corrosion rate of the pure Ti foam (0/100 HA/Ti) and the FGM composite (10/90 HA/Ti) samples in a simulated body fluid (SBF). The results showed that the hardness of FGM composites, despite being less than that of 0/100 HA/Ti, was still within safe limits. The corrosion rate, however, was found to be decreased by a significant value of almost 40% for the 10/90 HA/Ti FGM composite sample compared to the pure Ti foam control sample. It was concluded that the optimum composition 10/90 HA/Ti sample offers improved corrosion resistance while maintaining a sufficient allowable hardness level.

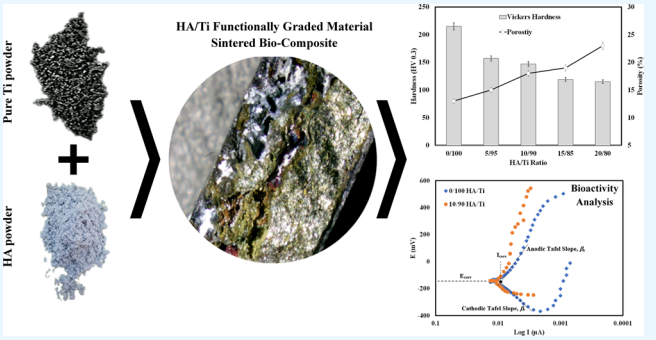

1. INTRODUCTION

Bone is a vital organ, and it is considered among the most frequently transplanted tissues of the human body. There has been a lot of research going on in the field of biomaterials to find the right combination of materials that could exactly mimic the natural tissue response upon implantation, providing a successful regeneration of the damaged tissue.[1] Biomaterials can be made from a wide range of materials, including metals, polymers, ceramics, and natural substances, such as bone and collagen.[2] Some examples of materials used as bone implants are metallic implants,[3] of which the most common metals used are Fe, Ni, Cr, Mn, Ti, and their intermixed alloys. Polymer implants made of polyethylene, polypropylene, and poly(vinyl chloride), for example, can be used to repair bones that have been damaged due to injury or disease. They are generally lighter than metal implants and can be molded into various shapes.[4,5] Similarly, natural biomaterials, such as bone and collagen, and ceramic implants of alumina and zirconia are strong and biocompatible.[6−8] These materials offer variable properties with respect to each other.

The importance of Ti and its alloys in biomedical applications has also been highlighted by numerous studies due to their superior toughness, biological inertness, increased electrochemical oxidation potential, and improved corrosion resistance.[9−11] Additionally, it has been proven that titanium and its alloys are risk-free and have no toxicological effects on humans.[12,13] Among ceramics, hydroxyapatite (HA) is considered to be one of the best bone substitutes. According to researchers, this naturally occurring calcium mineral accounts for 60% of the bone mass. Because of their chemical closeness to the mineral component of mammalian bones and teeth, calcium orthophosphates are commonly employed as bone substitute materials.[14] These materials are biocompatible,

Received: March 4, 2023
Accepted: July 21, 2023
Published: August 2, 2023

© 2023 The Authors. Published by American Chemical Society

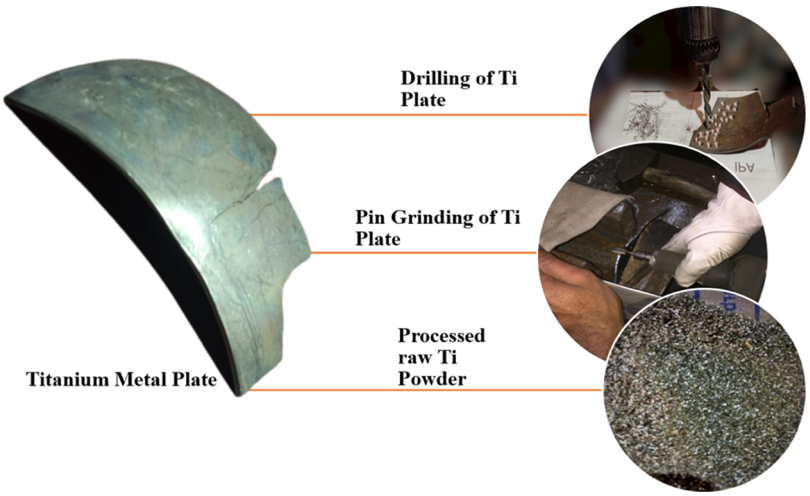

Figure 1. Production of Ti powder using drilling and pin grinding. Image on the left shows the Ti plate, being drilled in the top right image, followed by pin grinding in the next image, leading to Ti powder as shown in the bottom right.

Figure 2. Procedure to synthesize HA: (a) mixing of H_3PO_4 in a solution of $CaCO_3$ and water at a temperature of 80 °C with continuous stirring on a magnetic stirrer hot plate and allowing 4 h reaction time followed by (b) filtration to obtain HA powder and (c) dried HA.

nontoxic, and are not recognized as foreign materials in the body. Furthermore, they exhibit bioactive behavior and integrate into live tissue through the same processes that are engaged in the remodeling of healthy bones, resulting in an intimate physicochemical link between the implants and bone known as osseointegration. Calcium orthophosphates have also been discovered to promote osteoblast adhesion and proliferation, which are bone-forming cells. Given these characteristics, HA is widely recognized among the most effective materials for bone substitutes.[15] Its chemical makeup and biological function aid the implant's integration into living tissue, allowing it to develop a strong link with the bone. Owing to their excellent biocompatibility and capacity to encourage the proliferation of bone-forming cells, calcium orthophosphates are frequently used in biomedical applications.[16,17]

Similarly, poly(vinyl alcohol) (PVA) is a synthetic polymer that is widely utilized as a binder in a wide range of scientific applications.[18] Its aqueous solubility, biodegradability, strong binding strength, low toxicity, adaptability, and ease of usage make it extremely useful. One of the primary advantages of PVA as a binder is its high water solubility. This makes it a great choice for operations involving the use of water as a solvent, as it dissolves easily and generates a constant, homogeneous solution capable of binding a wide range of compounds together. It is also biodegradable, which means that it can be broken down into harmless molecules by natural processes. This makes it a friendly solution for biomaterial research applications.[19,20] It also has a high binding strength, making it a good choice for applications requiring a strong, long-lasting bond. Its low toxicity and easy handling make it a potential candidate for biological applications where biocompatibility is a high issue.

In this work, all major classes of biocompatible materials were used to obtain a customized functionally graded material (FGM) that could act as a possible replacement for conventional bone implants. The main idea was to develop a gradient structure in terms of porosity and chemical composition using a metallic foam substrate. A gradient structure helps reduce the metallic surface of the implant, which, in turn, can prevent many defects such as osteolysis (erosion and degradation of bone), aseptic loosening (loosening of joints and failure of bone and implant fusion), and elastic modulus mismatch. Furthermore, such a structure with a uniform porosity gradient presents a suitable site for growing bone tissue that can increase the rate of osteointegration.[9]

Development of HA/Ti bioimplants has recently been the subject of many investigations, where authors have proposed various fabrication routes, such as powder metallurgy,[21] electrophoretic deposition,[22,23] vacuum spray method,[24] plasma spray coating,[25] laser cladding,[26] etc. In this work, the powder metallurgy route was adopted for its cost effectiveness and ease of application as no special equipment or tooling is required. Three different metallic, ceramic, and polymeric materials used in this study were Ti, HA, and PVA, respectively. Ti was a material of choice for metal foam because of its excellent mechanical performance and low elastic modulus. HA is known to exhibit excellent support for bone

https://doi.org/10.1021/acsomega.3c01471
ACS Omega 2023, 8, 28976−28983

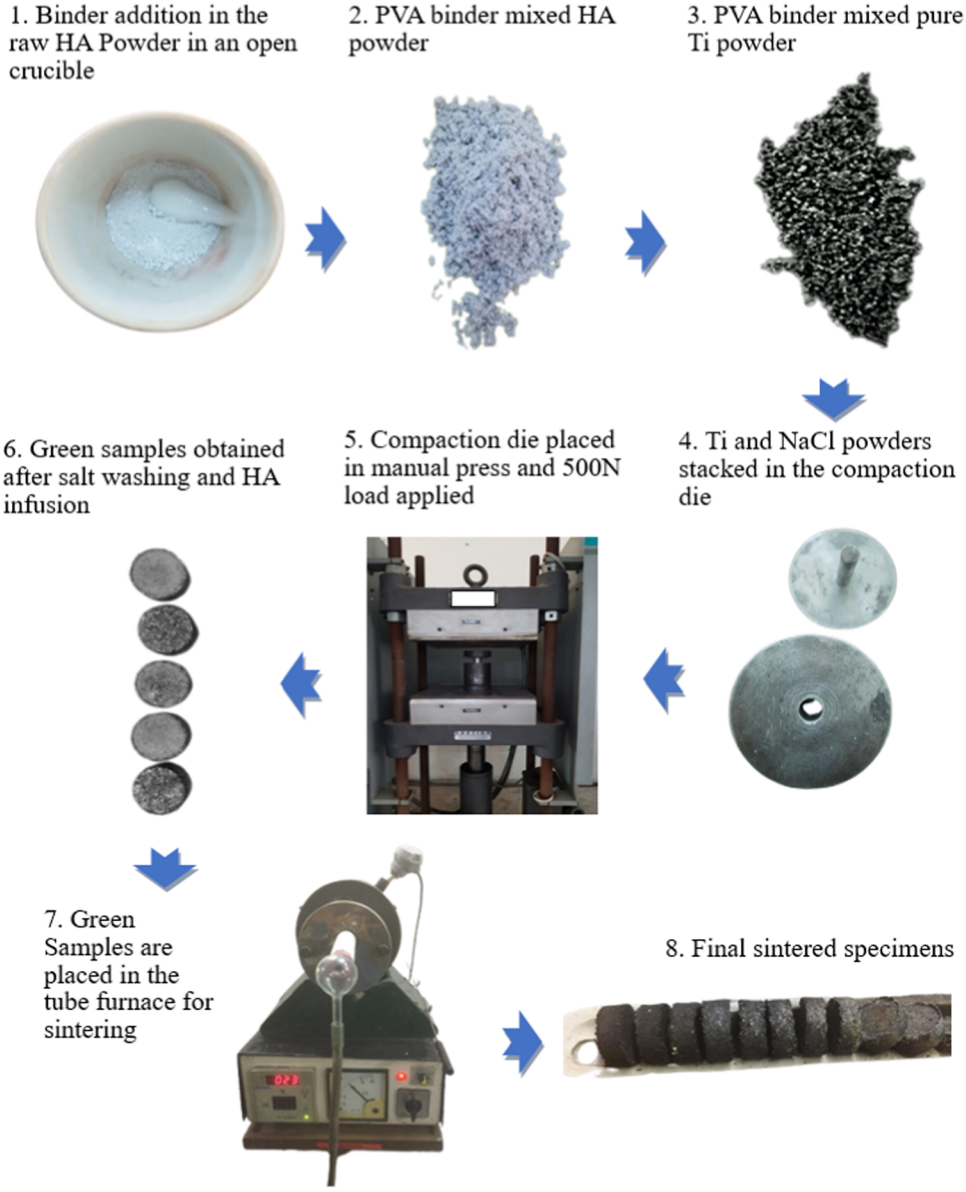

Figure 3. Process flow chart to produce FGM samples through powder metallurgy. First, the raw powders were mixed with a binder and dried. Next, Ti and space holder (NaCl) were stacked and compacted in a compaction die. Green compacts were then cleared of NaCl and infused with HA. Finally, the samples were sintered.

restoration and can increase the biocompatibility of the implant material to a great extent. It is also helpful for decreasing the metallic ion release by decreasing the contact of the metallic implant and bone. The polymeric material, i.e., PVA, used in the experiments was intended to facilitate the binding of both metal and ceramic.

2. EXPERIMENTAL WORK

2.1. Raw Materials. The raw materials used in the experiment included a commercially pure Ti metal plate, PVA binder, $CaCO_3$, and H_3PO_4, which were obtained from AF Corporation, Lahore, Pakistan, and Premier Quality Chemicals, Sheikhupura, Pakistan. These raw materials were processed to obtain final powders of Ti metal and HA. Ti powder production is illustrated in Figure 1, where a Ti plate was first drilled and then ground to yield metallic powder of 9−13 μm size.

HA was prepared by one-step synthesis of Ca-HA. It was done by mixing $CaCO_3$ in water heated to 80 °C in a liquid−solid ratio of 4.5, followed by slow addition of H_3PO_4 at a rate of 1 mL/min. The molar ratio of calcium to phosphorus was maintained at around 1.67. After 4 h reaction time, the mixture obtained was filtered and dried in an oven at 105 °C to be used as HA. The final product was obtained in a size range of 25−120 μm. The processing steps of HA powder are illustrated in Figure 2.

2.2. Sample Preparation. Ti and HA powders were mixed with a predetermined amount of PVA binder and water in separate crucibles. After a uniform mix was obtained, the binder-mixed Ti was placed in the open air to dry for 10−15 min. Multiple portions of Ti powder and NaCl were stacked up, with the space holder amounts ranging from 2 to 20%. The space holder used varied in size from 40 to 50 μm. The Ti/NaCl stacks were pressed using a manual hydraulic press in a die at an applied load of 500 N and a dwell time of 3 min to

https://doi.org/10.1021/acsomega.3c01471
ACS Omega 2023, 8, 28976−28983

ensure good green strength. The green compacts were then washed thoroughly to wash away NaCl and leave porosity for the infusion of HA. The porous green compacts were packed in the binder-mixed HA powder prepared earlier and sintered at a temperature of 1200 °C in a tube furnace equipped with a temperature controller, for 2 h in an inert gas environment to prevent oxidation. The heating rate during sintering was maintained initially at 10 °C/min, which was later reduced to 5 °C/min near the maximum sintering temperature. To promote the interfacial bonding at the contact, an intermediate dwell time of 30 min at the temperatures of 500, 800, and 1000 °C was also used. Multiple samples were synthesized to ensure the repeatability of the whole process and the results. In addition, specimens of different porosities and HA fractions were also prepared to check the effect of each percentage on the mechanical properties of the biocomposite. The overall sequence of the powder metallurgical synthesis route is given in Figure 3.

2.3. Material Characterization. Physical and microstructure characterization was performed on the samples to evaluate their performance against existing materials that are currently being studied as bone implants, comparing their structural integrity and biocompatibility. Visual inspection was carried out at first after sectioning and grinding the sample to evaluate the interface development. A high-resolution 50 megapixel camera was used to capture the surface features for the purpose of close observation.

Bulk and true densities were evaluated for the samples using standards BSEN12390-7, B212-17, and D854-06. The bulk density of the material was calculated by taking a mass to volume ratio such that the overall volume of both the open and closed pores of the samples was included. On the other hand, the true density was estimated using the volume of the solid material in the sample only, i.e., excluding the open and closed pores. In this work, the true density was measured with the help of a pycnometer (Gay-Lussac, 50 mL, Cole-Parmer, IL) according to the ASTM D854-14 standard and using the equation given below

$$\text{true density} = \text{density of water} \times \frac{(M_2 - M_1)}{(M_2 - M_3)} \quad (1)$$

where

$$\text{weight of pycnometer} + \text{water} = M_1$$

$$\text{weight of pycnometer} + \text{water} + \text{sample weight outside} = M_2$$

$$\text{weight of pycnometer} + \text{water} + \text{sample weight inside} = M_3$$

The percentage porosity of each composition sample was calculated by using the formula

$$\%\ \text{porosity} = 1 - \frac{\text{bulk density}}{\text{true density}} + 100 \quad (2)$$

To validate the purity of the Ti metal, the elemental analysis of its powder was conducted using an X-ray fluorescence spectrometer (XRF, Baltic Scientific Instruments, Riga, Latvia).

Hardness of the samples was measured to evaluate their resistance to unified loads. It gives a good idea about the strength of the material. A Vickers hardness tester (Model: LECO DM-400T, Saint Joseph, MI) with a low-force range (0.3 HV) was used in accordance with the standard ASTM E92-17. This testing procedure requires polished samples, an optical measurement system, and a diamond indenter. The hardness of the material can then be calculated by measuring the width of the indent.

The samples' surface morphology and porosity distribution were examined using a TESCAN MAIA3 field emission scanning electron microscope (FE-SEM) equipped with an Octane Elite EDAX detector (Brno-Kohoutovice, Czech Republic). Scanning was carried out using a secondary electron detector in a high vacuum at 12.5 kV acceleration voltage, with no sputter coating on any sample.

Finally, the corrosion analysis was performed on the 0/100 HA/Ti control sample and the 10/90 HA/Ti FGM composite sample to demonstrate the surface activity of each. This test was performed on a Gamry potentiostat, model: PCI/750 potentiostat/ZRA, Gamry Instruments, Warminster, PA. The standard ASTM G102 is typically used to calculate the corrosion rate in mm/year as per the following equation

$$\text{corrosion rate} = \frac{i_{\text{corr}} K E_{\text{w}}}{\rho A} \quad (3)$$

where E_{w}, ρ, and A are the equivalent weight in g/mol, the density in g/cm^3, and the surface area in cm^2, respectively, of the sample. The ASTM constant, K, has a value of 3272 mm/(A·cm·year·mol), while the corrosion current density, i_{corr}, in μA/cm^2, may be defined in terms of the polarization resistance, R_{p}, in Ω·cm^2, and the Tafel anodic (β_{a}) and cathodic (β_{c}) slopes in V/decade, using the Stern−Geary equation

$$i_{\text{corr}} = \frac{\beta_{\text{a}}\beta_{\text{c}}}{2.303(\beta_{\text{a}}\beta_{\text{c}})R_{\text{p}}} \quad (4)$$

The corrosion behavior of Ti and HA-infused samples was examined at 37 °C using a three-electrode cell in a simulated body fluid (SBF) solution maintaining the pH of 7.4. To perform this test, samples were first embedded in cold curing epoxy resin, exposing the surface area of 1 cm^2 only, followed by connecting it to the working electrode. A saturated calomel electrode and a graphite electrode served as the reference and counter electrodes, respectively. The chemicals and their composition used in SBF are reported elsewhere.[27]

3. RESULTS AND DISCUSSION

3.1. Visual Analysis, Densification, and Composition. High-magnification images were taken after sectioning the specimens, which revealed the interface clearly, as shown in Figure 4. Each layer of the material can be clearly distinguished, such as a seamless layer of pure Ti, perfectly sintered, followed by the layer of metallic foam, resulting due to the incorporation of salt as a placeholder. The image also illustrates that the placeholder is completely washed off, as is obvious from the presence of porosity in the sample. Lastly, the white regions of the figure identify the presence of HA infused deeply into the sample. Here, it should be noted that the HA is not present at the top or bottom surfaces. This is because it was removed to perform further testing on the sample. It was observed from the analysis of Figure 4 that the samples have good structural integrity and are free of cracks.

Figure 5 compares the bulk and true densities and porosity fractions of all the test samples. Table 1 reports a total of five compositions of HA/Ti samples that were compared with each

https://doi.org/10.1021/acsomega.3c01471
ACS Omega 2023, 8, 28976−28983

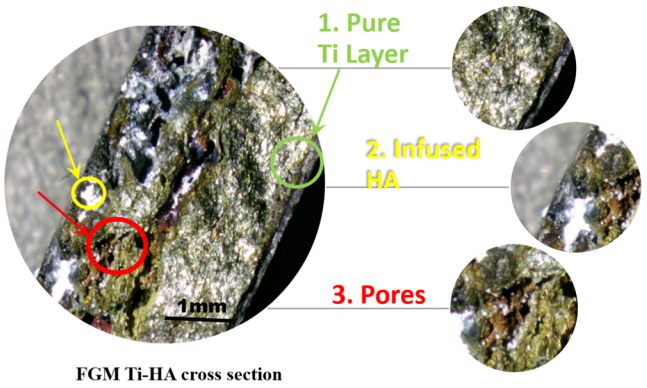

Figure 4. Cross-section view of 10/90 sample. The green, yellow, and red arrows represent the pure Ti layer, infused HA, and the porosity, respectively.

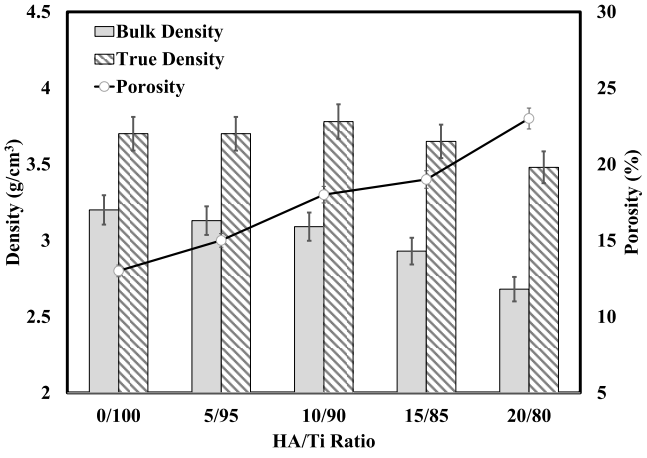

Figure 5. Comparison between bulk density, true density, and porosity fraction as a function of the HA/Ti ratio.

Table 1. Summary of Sample Codes, Compositions, Bulk Densities, True Densities, and Porosity Volume Fractions

sample no.	Ti (vol %)	HA (vol %)	HA/Ti	bulk density (g/cm^3)	true density (g/cm^3)	porosity (vol %)
1	100	0	0/100	3.20	3.70	13
2	95	5	5/95	3.13	3.70	15
3	90	10	10/90	3.09	3.78	18
4	85	15	15/85	2.93	3.65	19
5	80	20	20/80	2.68	3.48	23

other with respect to their densities in the final sintered state. Note that the true density for the sample 10/90 HA/Ti (HA: 10 vol %, Ti: 90 vol %) was observed to be maximum, which indicates better sintering and infusion of HA.

XRF analysis verified the purity standard of Ti powder; see Table 2. The chemical composition verifies that having experienced all the processing stages, the powder did not develop any unwanted oxides and maintained its corrosion resistance.

3.2. Vickers Hardness. Table 3 reports the Vickers hardness values obtained for each sample, and Figure 6 compares the hardness of each sample with the porosity fraction of that sample. It may be observed that there exists an inverse relation between the sample hardness and the porosity fraction. Note that a significant decrease in hardness of almost

Table 2. Elemental Composition of the Processed Ti

elements	mass (%)
Ti	99.4
V	0.31
Cr	0.20
Fe	0.015
Ni	0.059
Pd	0.016

Table 3. Vickers Hardness Values for HA/Ti Samples at a Low-Force Range (0.3 HV)

sample no	HA/Ti	hardness (0.3 HV)
1	0/100	215
2	05/95	157
3	10/90	147
4	15/85	119
5	20/80	115

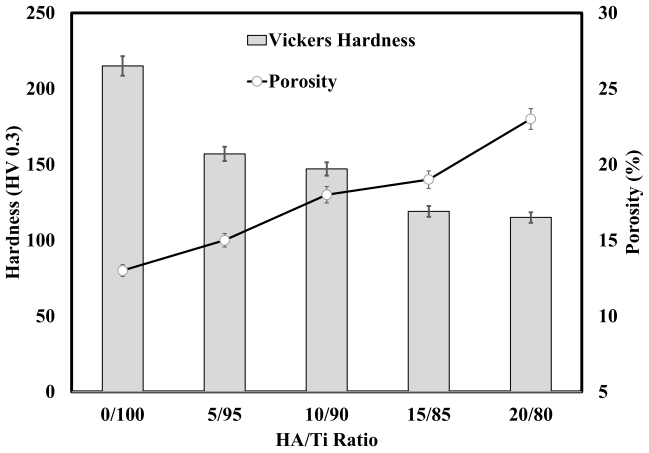

Figure 6. Comparison between Vickers Hardness and porosity fraction as a function of the HA/Ti ratio.

25% exists between the 0/100 HA/Ti control sample and 5/95 HA/Ti sample. This is due to the fact that the 0/100 HA/Ti control sample did not use any spacer material (NaCl) or impurity like HA during its compaction and sintering, and hence, a single-phase pure Ti powder led to better diffusion at the particle interface.

The hardness difference between 5/95 HA Ti and 10/90 HA Ti samples, however, was less than 5%. This suggests that with increasing volume fraction of the second phase particle, like HA, the decrease in hardness is essential. However, the higher level of true density after sintering, as was observed in the 10/90 HA/Ti sample, does not allow a rapid decrease in hardness. This finding is confirmed by the hardness values of 15/85 and 20/80 HA/Ti samples, where a sudden decrease in hardness was observed once again due to minimum bulk and true densities (see Figure 5).

Comparing the hardness values of the actual bone (~100 HV) with 0/100 HA/Ti and 10/90 HA/Ti composite samples, it is identified that the samples under consideration exhibited excellent results, with the corresponding hardness values almost twice that of the actual bone. This specifies that not only the pure Ti foam but also the 10/90 HA/Ti FGM composite exceeds the necessary standard for hardness.

3.3. Microstructural Analysis. SEM of the samples was performed on three different compositions, including 0/100,

https://doi.org/10.1021/acsomega.3c01471
ACS Omega 2023, 8, 28976−28983

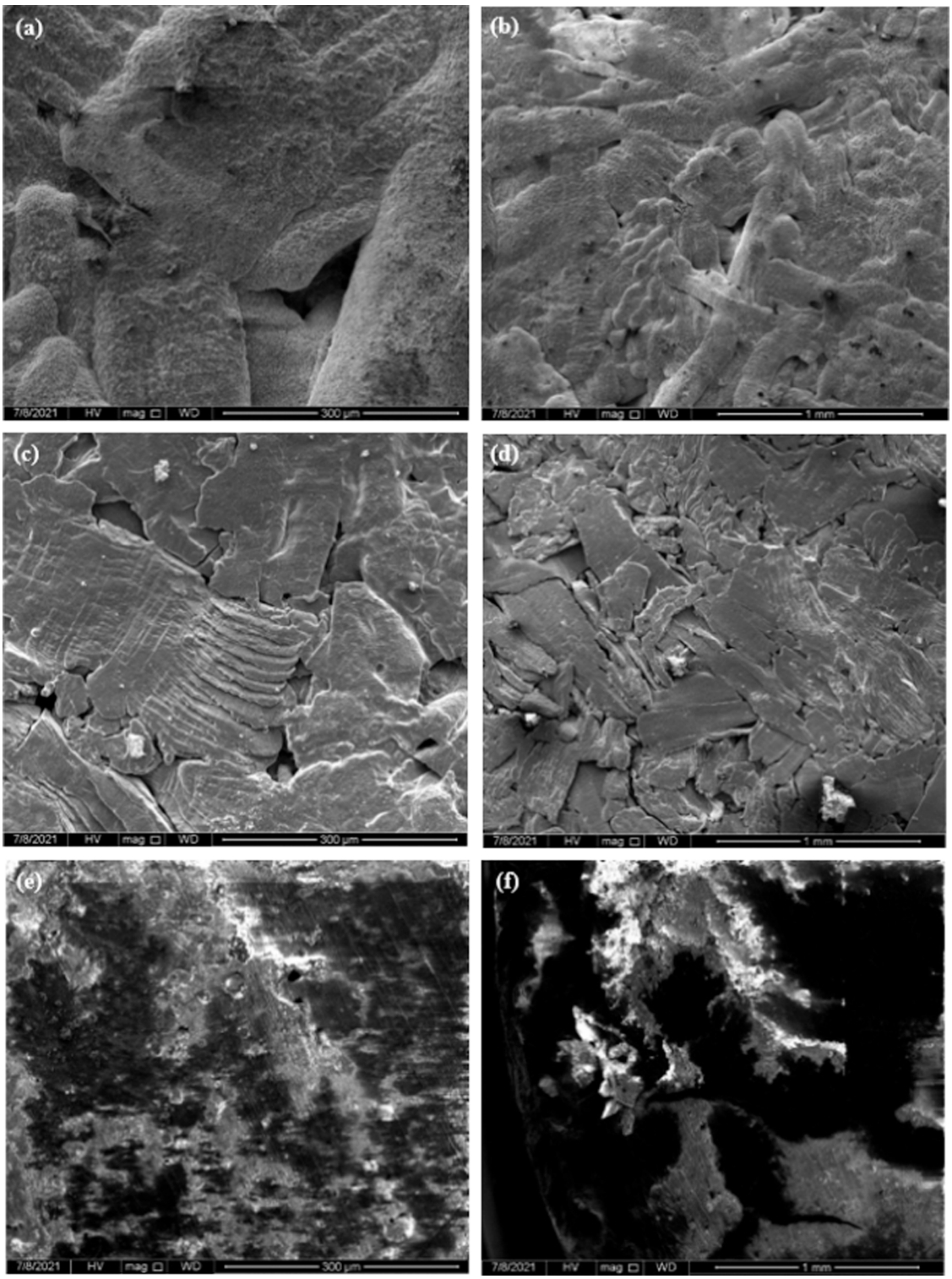

Figure 7. SEM images of 0/100 HA/Ti at (a) 500× and (b) 130×; 10/90 HA/Ti at (c) 500× and (d) 130×; and 20/80 HA/Ti at (e) 500× and (f) 130×.

10/90, and 20/80 HA/Ti, as shown in Figure 7. For the control sample with 100% Ti (Figure 7a,b), it was observed that the powder upon sintering was more fused showing lesser porosity and compacted due to its high purity, and hence, there was a greater possibility of interface development between the similar crystals. This was also confirmed earlier when the hardness value of the same sample was discussed in comparison to other composite samples. The 0/100 HA/Ti control sample was prepared to investigate the relative loss of strength and other properties by HA incorporation. At this stage, the particles were at the verge of third and fourth stage of sintering and almost lost their individual identity due to sintering, although a vague identification is still noticeable. However, as soon as the second phase HA was added, a more porous structure appeared in the micrographs mainly due to the different crystalline and chemical natures of the structures

https://doi.org/10.1021/acsomega.3c01471
ACS Omega 2023, 8, 28976−28983

(see Figure 7c,d). Similar observations were recorded for the samples with higher amounts of HA, such as 20/80 of HA/Ti (see Figure 7e,f). One obvious observation is that the visual difference of porosity between samples incorporated with HA is significant in comparison to the sample with pure Ti, which is also justifiable from the hardness data where reduction is drastic in a similar fashion among the composites discussed.

3.4. Corrosion Rate Analysis. Figure 8 illustrates the potentiodynamic polarization curves of 0/100 HA/Ti and 10/90 HA/Ti samples, where the former is the control sample and the latter is the FGM composite sample that showed promising results, as discussed previously, in terms of true density, sintered state, and hardness level. Table 4 summarizes the data acquired from Figure 8, including corrosion potential (E_{corr}) in mV, corrosion current density (i_{corr}) in $\mu A/cm^2$, polarization resistance (R_p) in $\Omega \cdot cm^2$, anodic (β_a) and cathodic (β_c) Tafel slopes in V/decade, and the corrosion rate in mm/year.

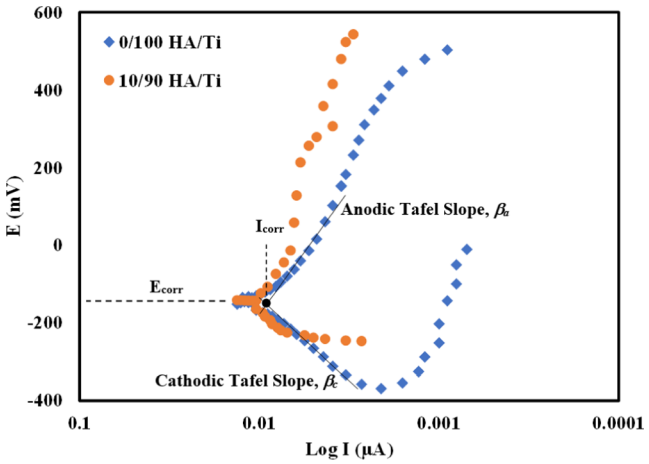

Figure 8. Potentiodynamic polarization curves of the 0/100 HA/Ti control and 10/90 HA/Ti FGM composite samples.

The estimated corrosion rates characterize the biocompatibility of the specimens by evaluating their electrochemical corrosion behavior. The results reveal that 10/90 HA/Ti has a lower corrosion current density and corrosion rate with a higher tendency for passivation compared to the control sample. Moreover, its shift to less negative potential indicates that the presence of HA on the Ti surface blocked the diffusion of ions from penetrating into the surface and hence restricted the corrosion rate of the underlying material to a great extent. It may, therefore, be stated that good chemical inertness of the HA/Ti FGM composite specimens was observed against SBFs and that the composite is likely to exhibit appreciable biocompatibility as a bioimplant.

4. CONCLUSIONS

In this work, a new FGM biomedical composite was synthesized by a very simple and economical method via powder metallurgy. The analysis of the samples depicted a porous structure containing micro- and macropores throughout the cross-section, as confirmed by SEM images and porosity volume fraction. The sintering of particles was well-diffused, resulting in a composite, in which HA particles were well integrated into the Ti matrix. The pores were meant to serve as a site for tissue growth and help prevent bone displacement.

From the results of true density and porosity fraction, the sample of optimum composition was found to be the 10/90 HA/Ti FGM composite. This sample also yielded relatively better hardness owing to the good compaction and sintering. It can be concluded from the corrosion rate analysis that 10% addition of HA to the porous Ti substrate leads to a significant 40% decrease in the corrosion rate at the expense of almost 25% loss in hardness. Nevertheless, the hardness value (147 HV) of the composite still lies within the acceptable hardness range, i.e., between pure Ti foam (~250 HV) and mammalian bone (~100 HV). This implies that the 10/90 HA/Ti FGM composite is almost twice as hard as a human bone. Lastly, the bioactivity test, as evaluated by the potentiodynamic polarization potentials of 0/100 and 10/90 HA/Ti, showed very little pitting or salt formation, which, in turn, suggested that the pure Ti foam and 10/90 HA/Ti FGM composite are both equally biocompatible.

AUTHOR INFORMATION

Corresponding Author

Muhammad Zain-ul-Abdein − *Department of Metallurgical and Materials Engineering (MME), Faculty of Chemical, Metallurgical and Polymer Engineering, University of Engineering and Technology (UET), Lahore 54890, Pakistan*; orcid.org/0000-0002-5754-6667; Phone: +92 42 99029207; Email: mzainulabdein@gmail.com; Fax: +92 42 99250202

Authors

Ehsan Ul Haq − *Department of Metallurgical and Materials Engineering (MME), Faculty of Chemical, Metallurgical and Polymer Engineering, University of Engineering and Technology (UET), Lahore 54890, Pakistan*

Furqan Ahmed − *Department of Metallurgical and Materials Engineering (MME), Faculty of Chemical, Metallurgical and Polymer Engineering, University of Engineering and Technology (UET), Lahore 54890, Pakistan*

Faseeh U Rehman − *Department of Metallurgical and Materials Engineering (MME), Faculty of Chemical, Metallurgical and Polymer Engineering, University of Engineering and Technology (UET), Lahore 54890, Pakistan*

Iftikhar Ahmed Channa − *Department of Metallurgical Engineering, NED University of Engineering and Technology, Off University Road, Karachi 75270, Pakistan*

Muhammad Atif Makhdoom − *Institute of Metallurgy and Materials Engineering, University of the Punjab, Lahore 54590, Pakistan*

Junaid Shahzad − *Department of Metallurgical and Materials Engineering (MME), Faculty of Chemical, Metallurgical and Polymer Engineering, University of Engineering and Technology (UET), Lahore 54890, Pakistan*

Table 4. Data Obtained from Potentiodynamic Polarization Curves for 0/100 HA/Ti and 10/90 HA/Ti Samples

sample	E_{corr} (mV)	i_{corr} ($\mu A/cm^2$)	β_a (V/decade)	β_c (V/decade)	R_p ($\Omega \cdot cm^2$)	corrosion rate (mm/year)
0/100 HA/ Ti	−153.0	1.45	0.249	0.431	47301.43	0.0252
10/90 HA/Ti	−143	0.91	0.104	0.115	26058.63	0.0158

https://doi.org/10.1021/acsomega.3c01471
ACS Omega 2023, 8, 28976−28983

Tooba Shafiq − *Department of Metallurgical and Materials Engineering (MME), Faculty of Chemical, Metallurgical and Polymer Engineering, University of Engineering and Technology (UET), Lahore 54890, Pakistan*
Muhammad Ali Shar − *Department of Mechanical & Energy Systems Engineering, Faculty of Engineering and Informatics, University of Bradford, Bradford BD7 1DP, U.K.*
Abdulaziz Alhazaa − *Department of Physics and Astronomy, College of Science, King Saud University, Riyadh 11451, Saudi Arabia*

Complete contact information is available at:
https://pubs.acs.org/10.1021/acsomega.3c01471

Notes

The authors declare no competing financial interest.

■ ACKNOWLEDGMENTS

The authors would like to acknowledge the Researcher's Supporting Project Number (RSP2023R269), King Saud University, Riyadh, Saudi Arabia, for their support in this work.

■ REFERENCES

(1) Patty, D. J.; Nugraheni, A. D.; Ana, I. D.; Yusuf, Y. Mechanical Characteristics and Bioactivity of Nanocomposite Hydroxyapatite/Collagen Coated Titanium for Bone Tissue Engineering. *Bioengineering* **2022**, *9*, No. 784.
(2) Walter, N.; Stich, T.; Docheva, D.; Alt, V.; Rupp, M. Evolution of Implants and Advancements for Osseointegration: A Narrative Review. *Injury* **2022**, *53*, S69−S73.
(3) Ahmed, F.; Zain-ul-abdein, M.; Channa, I. A.; Yaseen, M. K.; Gilani, S. J.; Makhdoom, M. A.; Mansoor, M.; Shahzad, U.; Jumah, M. N. b. Effect of Ultrasonic Surface Mechanical Attrition Treatment-Induced Nanograins on the Mechanical Properties and Biocompatibility of Pure Titanium. *Materials* **2022**, *15*, No. 5097.
(4) Auclair-Daigle, C.; Bureau, M. N.; Legoux, J.-G.; Yahia, L. Bioactive Hydroxyapatite Coatings on Polymer Composites for Orthopedic Implants. *J. Biomed. Mater. Res. A* **2005**, *73A*, 398−408.
(5) Kargupta, R.; Bok, S.; Darr, C. M.; Crist, B. D.; Gangopadhyay, K.; Gangopadhyay, S.; Sengupta, S. Coatings and Surface Modifications Imparting Antimicrobial Activity to Orthopedic Implants. *Wiley Interdiscip. Rev.: Nanomed. Nanobiotechnol.* **2014**, *6*, 475−495.
(6) M, K.; H, A. Bone Graft Substitutes for Bone Defect Regeneration. A Collective Review. *Int. J. Dent. Oral Sci.* **2014**, 247−255.
(7) Barabashko, M.; Ponomarev, A.; Rezvanova, A.; Kuznetsov, V.; Moseenkov, S. Young's Modulus and Vickers Hardness of the Hydroxyapatite Bioceramics with a Small Amount of the Multi-Walled Carbon Nanotubes. *Materials* **2022**, *15*, No. 5304.
(8) Vaiani, L.; Boccaccio, A.; Uva, A. E.; Palumbo, G.; Piccininni, A.; Guglielmi, P.; Cantore, S.; Santacroce, L.; Charitos, I. A.; Ballini, A. Ceramic Materials for Biomedical Applications: An Overview on Properties and Fabrication Processes. *J. Funct. Biomater.* **2023**, *14*, No. 146.
(9) Babaie, E.; Bhaduri, S. B. Fabrication Aspects of Porous Biomaterials in Orthopedic Applications: A Review. *ACS Biomater. Sci. Eng.* **2018**, *4*, 1−39.
(10) Jawed, S. F.; Rabadia, C. D.; Khan, M. A.; Khan, S. J. Effect of Alloying Elements on the Compressive Mechanical Properties of Biomedical Titanium Alloys: A Systematic Review. *ACS Omega* **2022**, *7*, 29526−29542.
(11) Zain-ul-Abdein, M.; Ahmed, F.; Durst, K.; Ali, M.; Daraz, U.; Khan, A. A. Coating delamination analysis of diamond/Ti and diamond/Ti-6Al-4V systems using cohesive damage and extended finite element modeling. *Surf. Topogr.: Metrol. Prop.* **2021**, *9*, No. 035034.
(12) Torres, Y.; Pavón, J. J.; Rodríguez, J. A. Processing and Characterization of Porous Titanium for Implants by Using NaCl as Space Holder. *J. Mater. Process. Technol.* **2012**, *212*, 1061−1069.
(13) Radovanović, M. B.; Tasić, Ž. Z.; Simonović, A. T.; Mihajlović, M. B. P.; Antonijević, M. M. Corrosion Behavior of Titanium in Simulated Body Solutions with the Addition of Biomolecules. *ACS Omega* **2020**, *5*, 12768−12776.
(14) Dorozhkin, S. Calcium Orthophosphate-Containing Biocomposites and Hybrid Biomaterials for Biomedical Applications. *J. Funct. Biomater.* **2015**, *6*, 708−832.
(15) Dudek, A.; Adamczyk, L. Properties of Hydroxyapatite Layers Used for Implant Coatings. *Opt. Appl.* **2013**, *43*, 143−151.
(16) Dorozhkin, S. V. Calcium Orthophosphate-Based Biocomposites and Hybrid Biomaterials. *J. Mater. Sci.* **2009**, *44*, 2343−2387.
(17) Dorozhkin, S. V. *Calcium Orthophosphate-Based Bioceramics and Biocomposites*; Wiley Online Library, 2016.
(18) Dong, R.; Pang, Y.; Su, Y.; Zhu, X. Supramolecular Hydrogels: Synthesis, Properties and Their Biomedical Applications. *Biomater. Sci.* **2015**, *3*, 937−954.
(19) Comyn, J. *What Are Adhesives and Sealants and How Do They Work? In Adhesive Bonding: Science, Technology and Applications*, 2nd ed.; Adams, R. D., Ed.; Woodhead Publishing, 2021; pp 41−78.
(20) Polyvinyl alcohol adhesives. U.S. Patent US3668166A, 2023. (accessed April 10, 2023).
(21) Singh, G.; Sharma, N.; Kumar, D.; Hegab, H. Design, Development and Tribological Characterization of Ti−6Al−4V/Hydroxyapatite Composite for Bio-Implant Applications. *Mater. Chem. Phys.* **2020**, *243*, No. 122662.
(22) Khanmohammadi, S.; Ilkhchi, M. O.; Allafi, J. K. Electrophoretic deposition and characterization of bioglass-whisker hydroxyapatite nanocomposite coatings on titanium substrate. *Surf. Coat. Technol.* **2019**, *378*, No. 124949.
(23) Nuswantoro, N. F.; Juliadmi, D.; Fajri, H.; Manjas, M.; Suharti, N.; Tjong, D. H.; Affi, J.; Gunawarman, G. Electrophoretic Deposition Performance of Hydroxyapatite Coating on Titanium Alloys for Orthopedic Implant Application. *Mater. Sci. Forum* **2020**, *1000*, 69−81.
(24) Xu, J.; Aoki, H.; Kasugai, S.; Otsuka, M. Enhancement of mineralization on porous titanium surface by filling with nano-hydroxyapatite particles fabricated with a vacuum spray method. *Mater. Sci. Eng., C* **2020**, *111*, No. 110772.
(25) Hu, F.; Fan, X.; Peng, F.; Yan, X.; Song, J.; Deng, C.; Liu, M.; Zeng, D.; Ning, C. Characterization of Porous Titanium-Hydroxyapatite Composite Biological Coating on Polyetheretherketone (PEEK) by Vacuum Plasma Spraying. *Coatings* **2022**, *12*, No. 433.
(26) Chakraborty, R.; Raza, M. S.; Datta, S.; Saha, P. Synthesis and characterization of nickel free titanium−hydroxyapatite composite coating over Nitinol surface through in-situ laser cladding and alloying. *Surf. Coat. Technol.* **2019**, *358*, 539−550.
(27) Arthanari, S.; Nallaiyan, R. Surface characteristics, corrosion resistance and MG63 osteoblast-like cells attachment behaviour of nano SiO2−ZrO2 coated 316L stainless steel. *RSC Adv.* **2015**, *5*, 26007−26016.